Hindawi
Advances in Civil Engineering
Volume 2019, Article ID 8314543, 18 pages
https://doi.org/10.1155/2019/8314543

Research Article

Static Behavior of a Modified Through-Core Connection between CFST Column and Composite Beam

Qi-shi Zhou,[1] Hua-wei Fu,[1] Xu-hong Zhou,[2] Yu-jie Yu,[1] and Qian-ren Wang[1]

[1]*School of Civil Engineering, Central South University, Changsha, Hunan Province 410075, China*
[2]*School of Civil Engineering, Chongqing University, Chongqing 400045, China*

Correspondence should be addressed to Hua-wei Fu; huaweifu@csu.edu.cn

Received 10 September 2019; Revised 24 November 2019; Accepted 30 November 2019; Published 19 December 2019

Academic Editor: Paolo Castaldo

Through-core connection has been proven to be an ideal solution to ensure a rigid connection between steel beams and CFST columns. However, the traditional through-core connection sometimes encounters concrete filling problems. A modified through-core connection design with details of reduced flange width was therefore proposed. Through-core reinforcements were added as supplements for tension load transfer. The monotonic loading tests and comprehensive FE simulations were performed to investigate the load bearing performance and working mechanism of this modified connection. The results indicated that the modified through-core connection presented plasticity hinge failure at the beam end and crack formulation and progradation at the RC slab. The reduced flange width reduced the strength of the connection, but the reduction extent was limited. Due to the through-core construction, the majority of internal forces at the beam were directly transferred into the column. The through-core reinforcement can effectively participate in load bearing after the connection yields. The flange width reduction extent and the length of the reduction region must be controlled to ensure sufficient connection strength. The number of shear studs and TC reinforcements can influence the load bearing ability, and design suggestions are provided for the modified through-core connection.

1. Introduction

Concrete-filled steel tube (CFST) columns synthesize the advantages of steel tubes and compressed concrete and have been increasingly utilized in Asian and European countries due to their high strength and good ductility. In recent years, CFST columns, especially rectangular CFST columns, have been extensively used in high-rise buildings, especially in earthquake-prone areas. A critical feature that is directly related to the resilience and aseismic performance of CFST frame structures is the connection between the beams and columns, which is usually the joint for attaching I-shaped steel beams to CFST columns. In previous studies and practical applications, rigid connections often adopt direct welding details where the I-beams are connected to the CFST columns through direct welding. Different from the I-beam to wide flange column connection, the welded I-beam to rectangular CFST column connection often leads to the separation of the steel tube from the concrete core under tensile loads, resulting in early fracture failure. The reasons for these failure modes are mainly attributable to the load path in CFST column connections, where the tension load is in fact transferred from the steel beam to the out-of-plane bending of the column flange, and the panel zone behavior is also different in wide flange column connections due to the presence of two webs [1, 2]. Then, to stiffen the joint region, the welded I-beam to CFST column connections are often stiffened with stiffeners inside or outside the columns [3, 4] or external plates surround the junction region [5].

Except for the strengthened connections, researchers have also sought alternative or modified connection details that can ensure rigid and ductile connection. One connection design that is regarded as the ideal rigid connection between the I-beam and CFST column is the through-beam connection or through-core connection [6, 7]. The connection is characterized by a continued steel beam or steel

girder passing through the column. During the fabrication of the through-core connection, an I-shaped slot is created in the tube. The steel beam is passed through the tube, and then fillet is welded to the tube before concrete filling [8]. Previous comparative tests have proved that these through-core connections present good cyclic behaviors and the highest stiffness when compared to other stiffened connections [9]. The internal load from the steel beam can then firmly transfer into the column with continuous beam construction, and the stress concentration on the tube wall can be effectively alleviated. Several seismic tests have also proven that a through-core connection can provide good seismic performance and achieve the desired seismic design objective of a "strong column-weak beam" and "strong joint-weak member" scenario [10]. As a result, the through-core connection has been a well-received option for rigid connections of heavy steel beams to CFT columns in high seismic risk regions [11].

Despite the advantages in mechanical performance, the through-core connections also possess some practical shortcomings in through-beam construction. When the girder dimension is close to the column diameter, the flange part inside the tube may interfere with the concrete filling in the CFST column and thus weaken the load bearing and bending performance of the CFST column. To address this problem, Zhou et al. [12] proposed a modified through-core detail in which the flange width of the through girder within the column region was reduced to provide space for the concrete to pass as shown in Figure 1. However, in this way, the load transferring ability of the steel girder was reduced. Then, to make up the lost strength from the section reduction, several longitudinal reinforcements (through-core reinforcements, "TC reinforcements" for short) in the reinforced concrete (RC) slab were installed through the CFST columns and welded to the tube to supplement the load transfer. In a composite girder beam, the steel girder and the RC slab are integrated together through shear studs, and then the slab can share the part of the load transferring demand at the upper flange. Then, the upper flange can allow for a higher extent of width reduction, and through appropriate setting arrangements of steel girders, the reinforcements in RC slabs and the shear studs, the girder, and the RC slab can interact and reach a balanced load transferring ability.

Several exploratory seismic tests have been performed on these modified through-core connections, and the results have indicated that the modified connection configuration can maintain good seismic performance if the flange width reduction is controlled within a reasonable range [12]. However, quasi-static tests cannot effectively reflect the load bearing mechanism, and the design guidance of the modified through-core connection still requires more in-depth investigation. Therefore, in this paper, a dedicated investigation has been performed on the static behavior of the modified through-core connection. Monotonic loading tests were initially conducted. Then, based on the test data, rational FE models of the modified connections were established and verified. Based on the test data and numerical simulations, the internal stress distributions, the internal force transferring patterns, and the cooperative working mechanisms between the assembled parts were all studied and discussed. Then, parametric studies were performed to investigate the influencing patterns of other connection details, such as flange width reduction degree, longitudinal length of flange reduction, and the quantity of TC reinforcements, through FE analysis. The research results can offer some design suggestions for this type of connection.

2. Experimental Test Program

2.1. Test Specimens. A total of four full-sized specimens (labeled CFCJ1~CFCJ4) were tested. The modified through-core connection features the reduction of flange width for the convenience of concrete casting and the supplemented load transfer from TC reinforcements. Then, the reduction degree of flange width was selected as the main varying factor. Detailed specimen parameters are given in Table 1 and Figure 2. The nominal dimension of the CFST column is $400 \times 400 \times 12$ mm (height × width × thickness). Due to the strengthened mechanism from the RC slab to the upper flange, the steel girder had a narrowed upper flange. Then, the steel beam adopted a dimension of $H300 \times 150 \times 200 \times 8 \times 12$ mm (height × upper flange width × bottom flange width × web thickness × flange thickness).

The flange width was reduced within the PT region, which was extended outside the column by approximately 310 mm from the junction boundary. The upper flange had more width reduction than the bottom, with the reduction ratio of the bottom flange B ($B = 2b/200$) being approximately 0.73 times that of the upper flange A ($A = 2a/150$). From CFCJ1 to CFCJ4, the reduction extent of the upper flange changed from 0 to 0.6 with an interval of 0.2. The construction and TC reinforcement arrangements remained the same for the 4 specimens. The steel beam and the RC slab were connected firmly with steel studs (13×80@50 mm). The steel beam and TC reinforcements all completely passed through the steel tube and were connected to the square steel column with a fillet weld before the concrete was poured. This type of connection is often applied in high-strength buildings and features a high axial load ratio in the column. During the tests, the axial load ratio n was set as 0.43 times the ultimate bearing capacity of the column.

The compressive strength of concrete was obtained through standard cube tests, and the average measured strength was 50.4 MPa. The measured modules and Poisson's ratio of concrete materials were 3.19×10^4 MPa and 0.21, respectively. The mechanical properties of the steel plates, steel bars, and studs were also measured through standard tensile tests [13], and the measured properties are given in Table 2.

2.2. Experimental Setup and Loading Procedure. The connection specimens were designed to simulate the connection of a frame structure under lateral loads, and then the frame inflection points were assumed at the midspan of the beams and midheight of the columns. The specimens were made

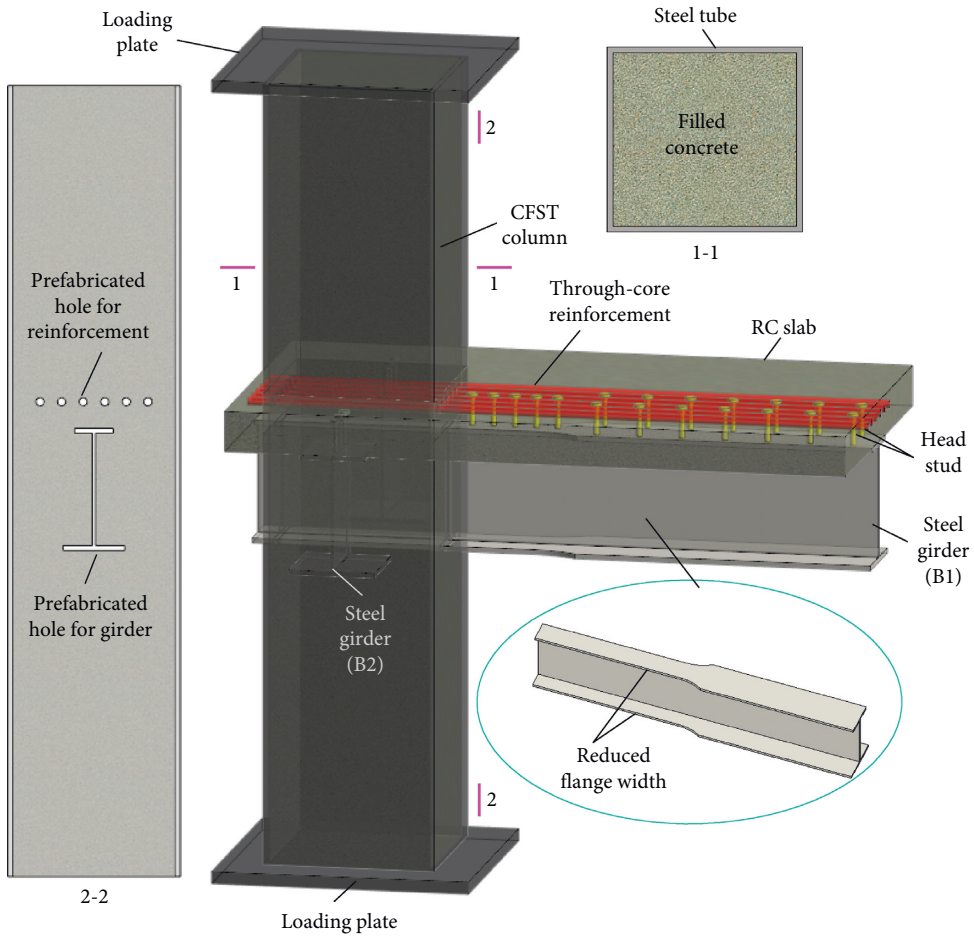

Figure 1: 3D schematic diagram of the specimens.

Table 1: Geometric details of specimens.

Specimen number	n	A/B	$a/b/R$ (mm)	TC reinforcement	Stud
CFCJ1	0.43	0/0	—/—/∞	6∅20@50	∅13 × 80
CFCJ2		0.2/0.146	15/14/233		
CFCJ3		0.4/0.292	30/28/139		
CFCJ4		0.6/0.438	45/42/111		

TC reinforcement—steel bar passing through the CFST column.

into T shape due to the setup limitations. Boundary conditions and loads of specimens are shown in Figure 3. The column ends were pin constraint at the lateral directions, and the monotonic force in the vertical downward direction was applied to the far end of the connected beam through stepwise loading process. Before the beam loading process, an axial force of 4000 kN (F1) is applied at the top cap of the column with the 20,000 kN actuator, and the load was kept constant throughout the entire testing process. This axial load level was determined based on the 0.43 axial load ratio and the axial bearing capacity 9270 kN of the CFST column calculated according to Chinese Code [14]. A two-stage loading process was adopted for the beam-tip loads (the distance of the loading point to the beam tip is 100 mm). A predicted yield load of the connection P_y was obtained through FE analysis prior the test, and the load-control loading method is applied at first during the initial loading period. This load-control protocol was continued until the specimen displayed yielding behaviors or the real-time load-displacement relation displayed obvious stiffness reduction. Then, the loading process was turned to displacement control, and the loading amplitudes were increased at an interval of displacement Δ at the moment of yielding. The test would be terminated when the applied load dropped below 85% of its peak value or the specimen can no longer be sustained. Strain gauges were used to measure the strains of the concerned locations in the steel components, through-core reinforcement, and the RC slab. Displacement meters and inclinometers are mounted to record the displacements and rotations. The detailed layout of the measuring apparatus is given in Figure 4.

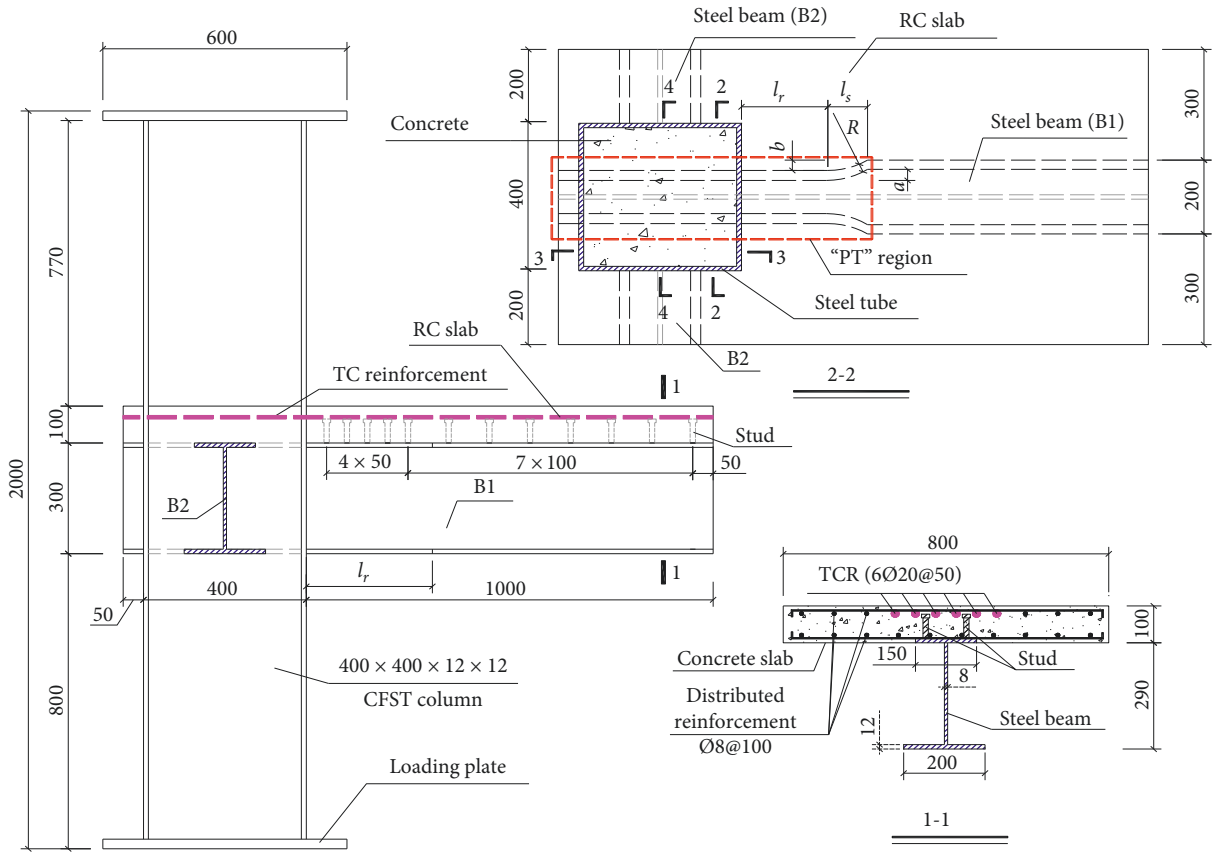

Figure 2: Details of specimens (units: mm).

Table 2: Mechanical properties of steel.

Type	Steel plate		Steel bars		Stud
Thickness or diameter (mm)	8	12	20	8	13
f_y (MPa)	310	300	485	300	380
f_u (MPa)	440	445	660	445	494
E_s (GPa)	208	203	211	209	210
ν_s	0.26	0.25	0.24	0.25	0.25

2.3. Results and Discussion. During the test, the CFCJ4 specimen failed early due to poor manufacturing quality, and the critical data (load and displacement) were not obtained due to fast degradation. Thus, only the CFCJ1 to CFCJ3 specimens were compared and discussed. The overall performance and failure modes of the three specimens were similar, and the entire monotonic load bearing process can be classified into four stages (S-1~S-4 in Figure 5):

(1) The first stage was the elastic period in which the relation of the vertical load versus displacement at the beam end was basically proportional. Every part of the connection stayed within the elastic state, and no cracks in the concrete slab were evident.

(2) The second stage started from the appearance of the first crack in the concrete slab (approximately 70 mm away from the column wall in all three specimens). During this stage, the applied vertical load still increased at a high rate as the beam end displacement increased, but the cracks in the RC slab continued to develop. The quantity and length of these cracks gradually increased as the beam-tip load increased, but no penetrating fracture was found. This stage stopped at the yielding of the connection, which was determined with the general yield moment method (GYMM) [15]. Then, at the end of this stage, slight buckling behaviors were presented at the lower flanges (such as CFCJ2 and CFCJ3 in Figure 6(a)). However, the web and the upper flange of the girder showed few visible deformations.

(3) The third stage was the plasticity development stage, in which the load bearing performance of the connection presented a plastic mode. During this stage, vertical displacement grew rapidly under the same increment of vertical load, and the stiffness of the connections decreased dramatically. During this stage, the buckling at the lower flanges became more severe, and slight deformation also appeared at the web region. During the latter period of this stage, the horizontal cracks in the RC slab penetrated throughout the entire range, and the cracking extent increased as the applied load increased (Figure 6(b)). The maximum crack width even reached 4 mm at the end of this stage. Slippage between the beam upper flange and the RC plate could also be observed to

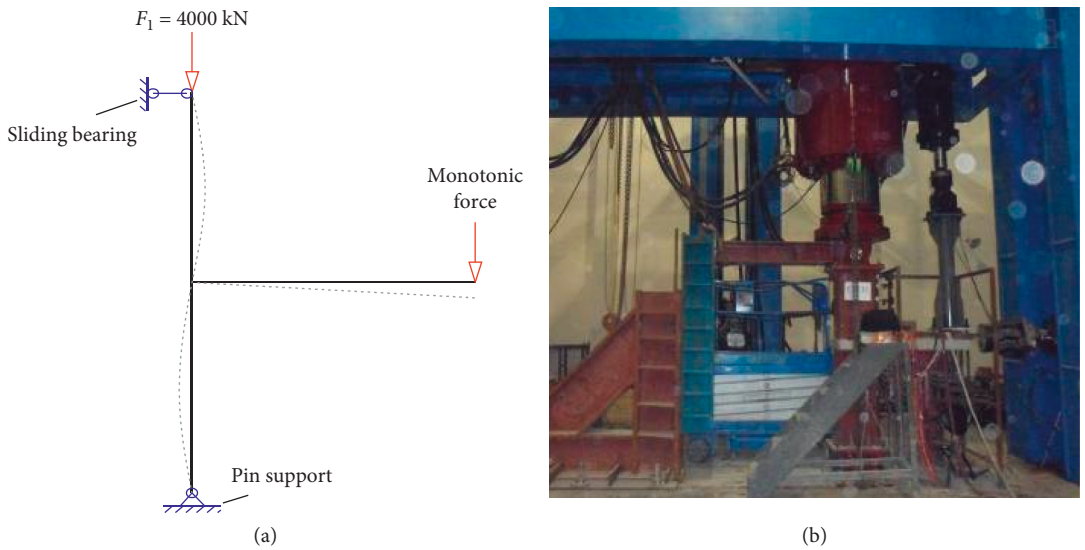

Figure 3: Mechanical model and test setup: (a) mechanical model; (b) photo of the test site.

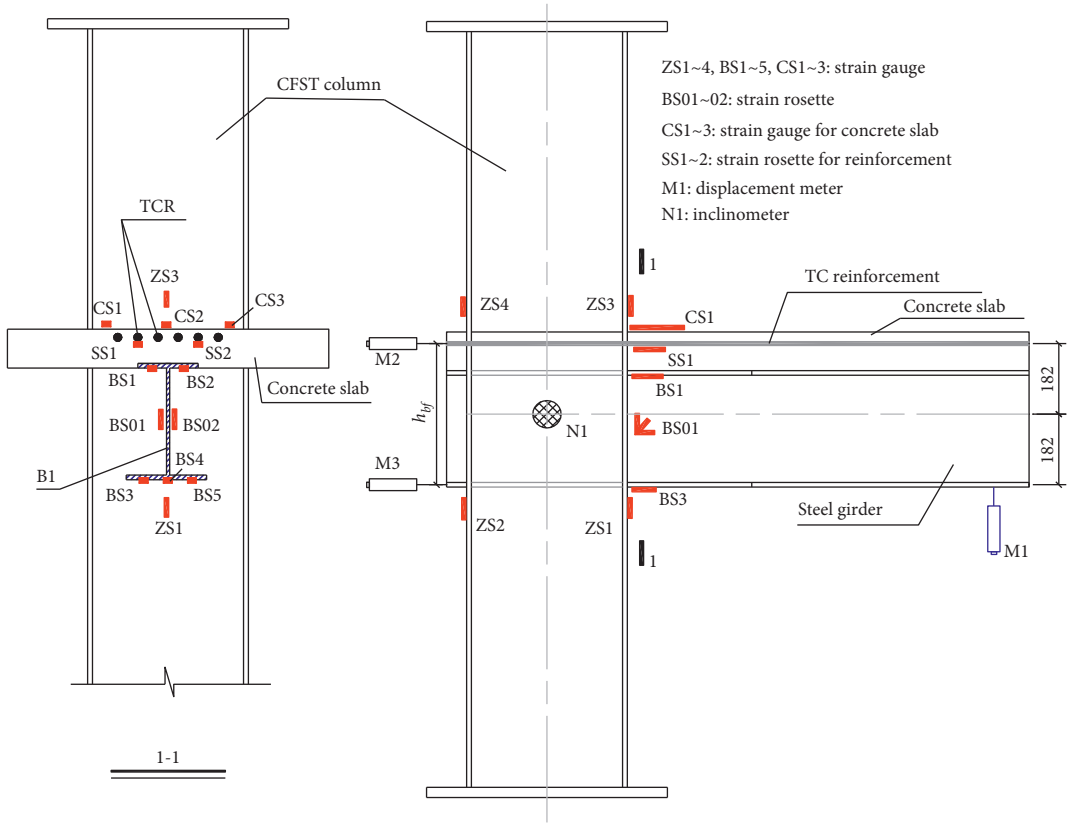

Figure 4: Arrangement of the measuring apparatus.

reach the maximum gradually, ranging from 2.0 mm to 3.5 mm, which relates to the maximal shear force between the beam upper flange and the RC plate.

(4) When the connection specimens reached the maximum load bearing ability, the specimens entered the fourth stage. This stage was the degradation stage and lasted until failure or the end of the test. During this stage, the bearing capacity of the joints declined continuously as the beam-tip displacement increased. The lower flange of the steel beam displayed local buckling and obvious plastic deformation. A few existing cracks in the RC slab almost penetrated (Figure 6(c)) the whole section. However, throughout the test, the CFST columns remained

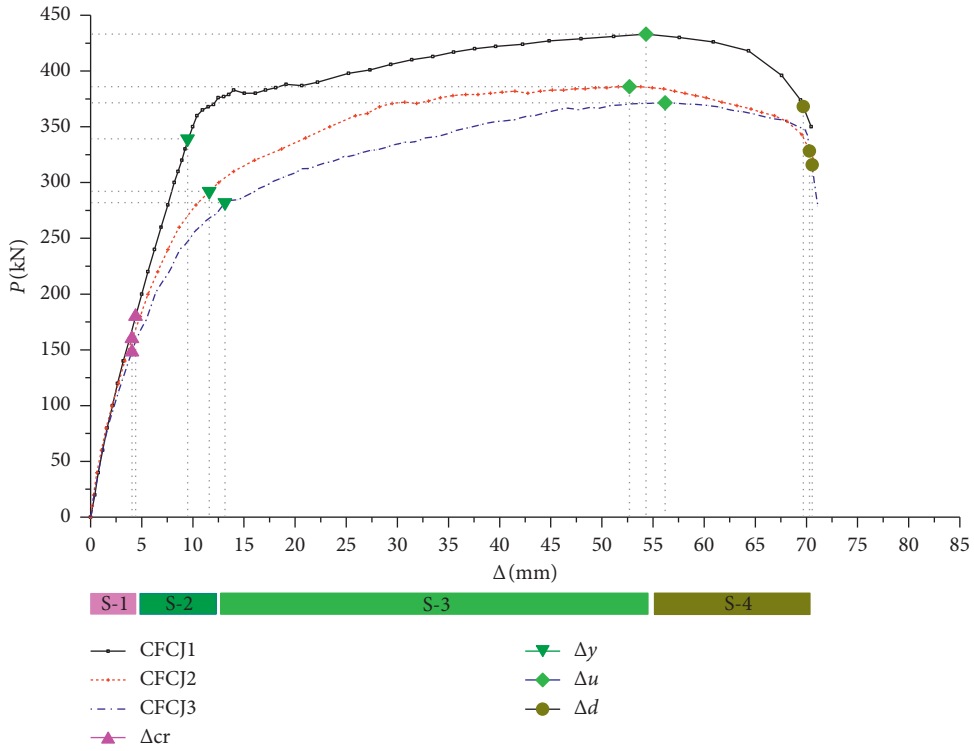

Figure 5: Beam-tip force versus beam-tip displacement curves.

intact without visible deformation, and the deformation and failure behaviors all occurred at the beam and slab regions.

Figure 5 shows the obtained applied load versus beam-tip displacement relations of CFCJ1–3. From CFCJ1 to CFCJ3, the steel girder had an increased extent of flange width reduction. Then, the connections displayed reduced stiffness and load bearing abilities. The CFCJ1 specimen had an intact steel girder and then displayed the highest stiffness and longer elastic region than the others. The reduced flange width led to reduced strength development and early plasticity development. A relatively large strength reduction was displayed between CFCJ1 and CFCJ2, but the difference between CFCJ2 and CFCJ3 was relatively small. This means that the extent of degradation decreased as the flange width decreased from 0.2 to 0.4. Table 3 lists the critical load and displacement at the boundary of adjacent stages, which were the crack moment (cr), yielding moment (y), ultimate strength moment (u), and fast-degraded moment (d). The comparison also indicated relatively more strength reduction between the intact connection and the 0.2 ratio reduction. However, the yield strength and ultimate strength of CFCJ2 and CFCJ3 still maintained more than 85% of the strength of CFCJ1.

3. Finite Element Models

To better obtain the working mechanism of the modified through-core connections, finite element models of the tested specimens were established using ABAQUS [16]. Following its validation with the experimental results, the internal stress stage and cooperative working mechanism during the loading process were discussed, and then a parametric study was performed using varying critical parameters in Section 4.

3.1. Element Types. Eight-node-reduced integral format 3D solid elements (C3D8R) were used to model the square steel column, steel beam, concrete slab, and loading plates. The truss element T3D2 was applied for the steel bars that were embedded in the concrete, and the truss elements were modified to be distributed in the RC slab in a discrete manner. A tie constraint that can couple two separated surfaces was used to simulate the welds between steel members, and no relative motion was allowed. The RC slab was bonded to the steel girder using shear studs. Then, in the FE model, the Timoshenko beam elements B31 were used to simulate the shear studs, and the interaction between the shear stud and the steel beam was simplified with the nonlinear spring elements ∗SPRING2 [12]. Then, during the model establishment process, the Beam-31 shear stud elements were positioned at the location of the shear studs and embedded into the concrete slab. Then, the shear studs were constrained to move together with the concrete slab. At the other end of the shear studs, a pair of zero-length spring elements was installed to connect the other end of shear studs and the corresponding node at the steel beam. Through this method, the interactions and the tensile force (spring-2 (V)) and shear force (spring-2 (H)) that transfer between the slab and girder were realized through the two direction spring elements. Figure 7(a) shows the meshed FE models, and Figure 7(b) shows the detailed settings of the spring

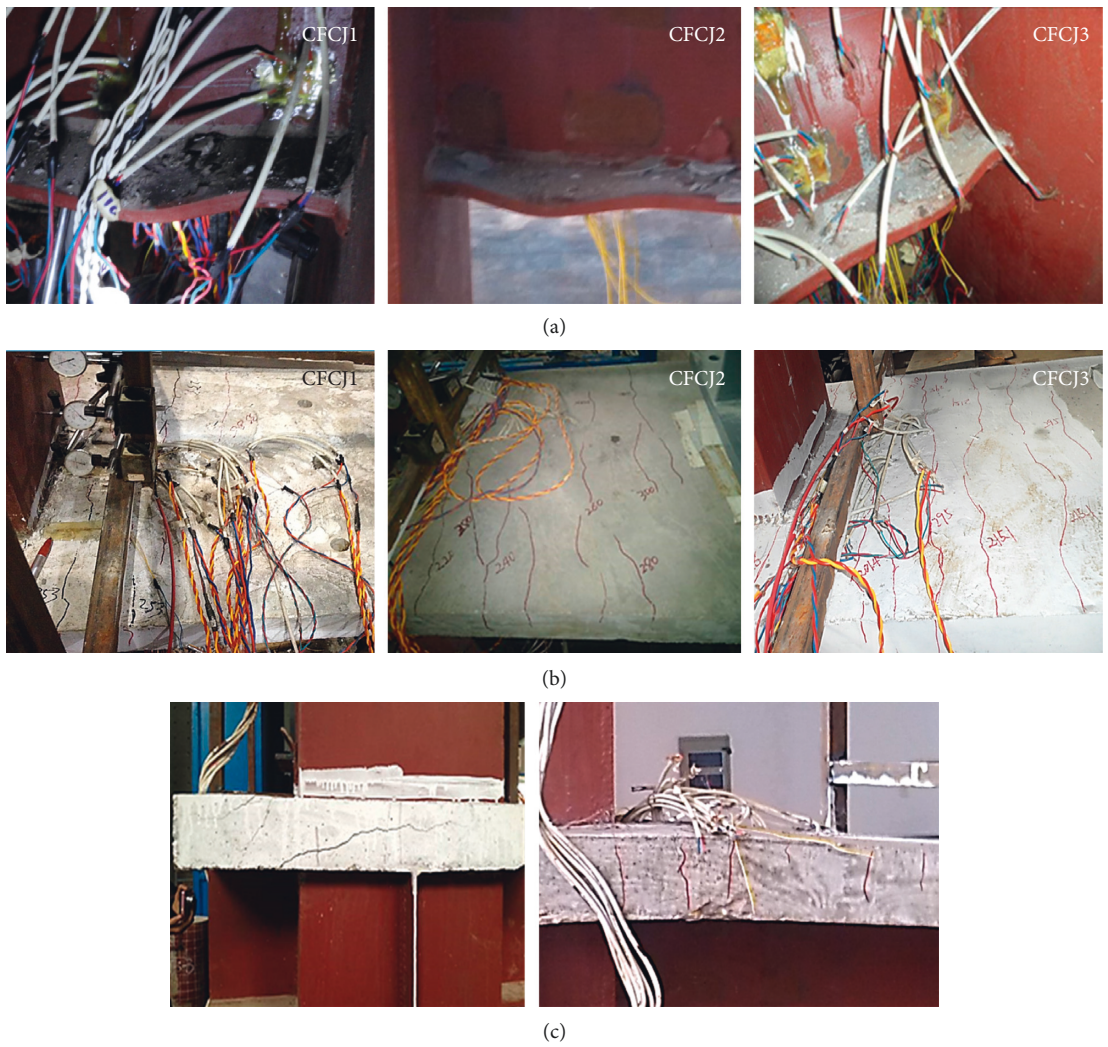

Figure 6: Failure modes observed for specimens CFCJ1~3: (a) local buckling in lower flanges; (b) surface crack distribution in RC slabs; (c) shape of penetrating cracks in RC slabs.

Table 3: Comparison of load at various stages.

	CFCJ1	CFCJ2	CFCJ3
P_{cr} (kN)	180	160	140
Δ_{cr} (mm)	8.2	10.3	10.8
P_y (kN)	380	342	323.6
Δ_y (mm)	16.1	18.67	19.63
P_u (kN)	433	384	371.6
Δ_u (mm)	54.3	45.8	56.2
P_d (kN)	396	322	214.6
Δ_d (mm)	67.6	68.1	72.2

elements at the shear connections. The mesh size was adjusted to satisfy a good accuracy and a reasonable computational time and was finally settled at approximately 25 mm for the joint region.

3.2. Boundary and Loading Conditions. The boundary and loading conditions were kept the same as in the test and are shown in Figure 7(a). Three reference points were assigned to the top and bottom surfaces of the CFST column and at the end surface of the beam. The kinematic coupling constraints in ABAQUS were adopted to connect the end surface to the corresponding reference point. Then, boundary constraints and point loads were applied to the reference points. The reference points at the bottom column end were constrained at the three directional displacements and the rotation freedom around the x-axis and z-axis. The top column end was restrained at the horizontal displacement freedom and the rotational freedom around the x-axis and z-axis. Therefore, only in-plane bending rotation was allowed. A constant axial load was initially applied on the top of the CFST column, and a vertical downward displacement load was applied at the tip point at the beam end.

3.3. Material Properties. The material constitutive model for steel and concrete adopted in this paper was suggested by Ding et al. [17]. A damaged plasticity model and the Willam–Warnke five-parameter failure criteria in ABAQUS were used to model the concrete material. An elastic-plastic model, considering von Mises yielding criteria, Prandtl–Reuss

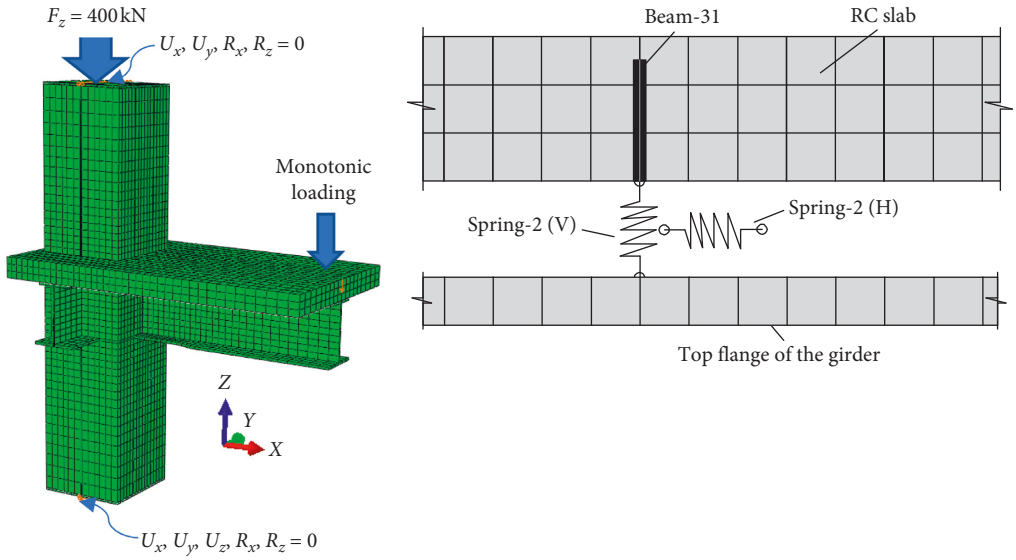

Figure 7: FE model: (a) typical meshing, boundary condition, and loading on the model of specimens; (b) modelling skill of a stud.

flow rule, and isotropic strain hardening, was applied to account for the steel constitutive behavior of the steel components. Detailed strengths were determined based on measured data in Table 2, and the parameter settings of the steel and concrete constitutive models can be found in reference [17]. The effectiveness of those constitutive models has been validated through a series of experimental studies [18, 19]. A trilinear model was applied to the shear stud material. The yield strength of the shear studs was 330 MPa, and the hardening modulus was taken as 0.01 E_{ss}, where E_{ss} is the elastic modulus of the shear stud modulus (2.06×10^5 MPa).

The stiffness value of spring-2 (V) was defined as 1×10^7 N/mm. The spring-2 (H) element obeyed the load-slip characteristics of the studs, and the lateral stiffness of the studs was determined with the load-slip relations that were proposed by Ollgaard et al. [20](equation (1)). The shear capacity of headed studs (P_u) can be calculated with equation (2):

$$\frac{P}{P_u} = \left(1 - e^{-0.71s}\right)^{0.4}, \tag{1}$$

$$P_u = 0.5A_s\sqrt{E_c f_c'} \le A_s f_u, \tag{2}$$

where S is the average slip and P is the shear force per stud. A_s is the cross-sectional area of the studs, E_c is the elastic modulus of the concrete, and f_c' is the cylinder compressive strength of the concrete. The Ollgaard theory assumes that P would reach 99% of the ultimate load P_u when the slip amount increases up to 5 mm. This lateral resistance-slip theory is also adopted in the latest steel structure design code-AISC 360 [21].

3.4. Contact. The surface-to-surface contact in ABAQUS was adopted to simulate the contact interactions between the steel and concrete (between steel beam and the RC slab and between steel tube and the infilled concrete). The "HARD CONTACT" mode was adopted for the nominal direction interaction, and the "Mohr–Coulomb friction model" with a friction coefficient of 0.6 was selected to simulate the tangential behaviors with referring related researches [22, 23].

4. Numerical Verification, Results, and Discussion

4.1. Load versus Displacement Relations. The comparison of beam end load versus displacement relations from the FE simulations and the test data are given in Figure 8. The comparison presents good agreement, and the FE models can effectively predict the elastic and plastic stiffnesses and the strength development and degradation process. Figure 9 gives the deformation conditions of each specimen at the moment of maximum strength. The four specimens also present obvious buckling deformation at the bottom beam flange, which corresponded well with the deformations observed in the tests (Figure 6(a)). The FE results indicated a higher level but a smaller buckling region at the beam end in CFCJ1. For the reduced flange specimens, the weaker flange led to an earlier and larger range of plasticity development, and then the buckling range increased.

4.2. Stress Characteristics. Figure 10 gives the stress conditions of the four tested specimens at the moment of maximum strength. Specimen CFCJ1–4 also displayed high stress at the TC reinforcements, indicating that the TC reinforcements can effectively participate in load bearing during hogging moment conditions. Due to the through-core construction, the high stresses at reinforcements outside the column range can effectively transfer into the column, and then the stress levels gradually decrease due to the load redistribution from the reinforcements to the infill concrete through concrete bonding. Under a vertical

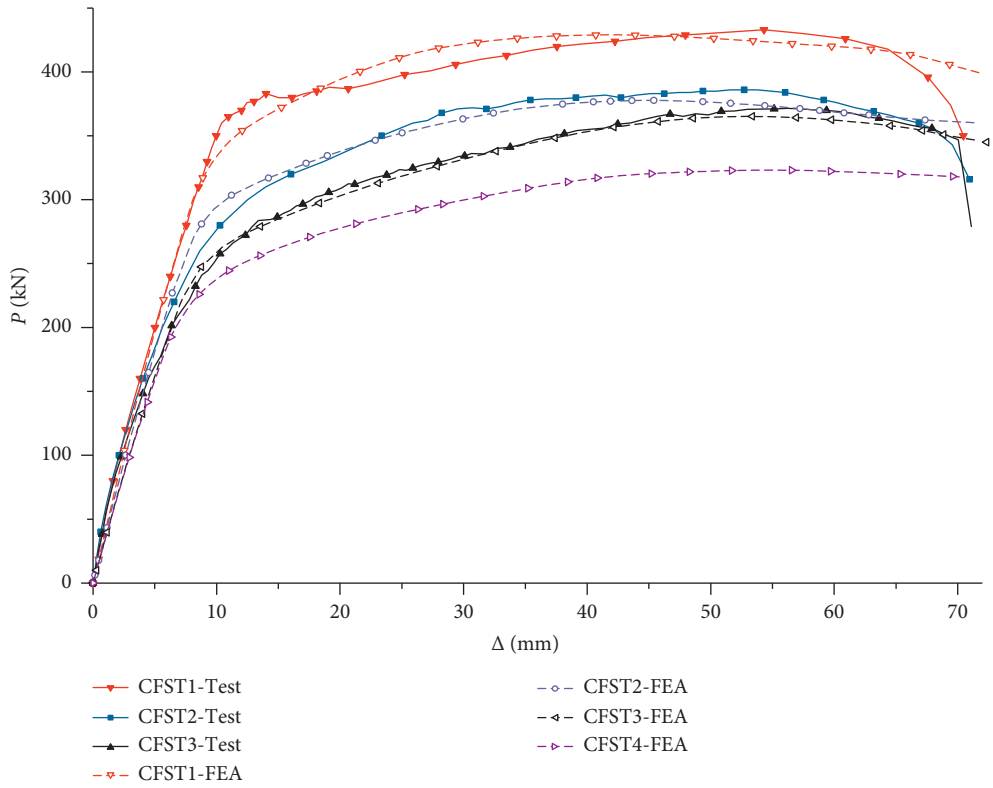

Figure 8: Comparison of FE analysis and experimental beam-tip force-displacement curves.

downward pushing load, the high stress first appeared at the bottom part of the beam web, where the plastic deformation and buckling behavior initiated.

Figure 11 shows the stress distribution of the junction region at the column flange. The results indicated that the reduction of flange width can influence the stress states at the column flange. As the extent of flange width reduction increased, the high stress region at the column flange first increased and then decreased. When the flange reduction extent changed from 0 to 0.4, the high-stress state only occurred at the bottom corner region above the bottom flange. When the flange width reduction extent was 0.6, a wider region of column flange presented high stresses, and the high stress region extended to regions around the bottom flange. However, the maximum stress at the column flange still did not exceed the yield point during the entire loading process. CFCJ1–4 had similar peak stress levels at the column flange, even with different flange reduction extents. This behavior indicated that the through-core connection mainly transfers the load through the continuous beam, not the bending of column flange.

Figure 12 shows the PEEQ (equivalent plastic strain) distribution at the core concrete, which can represent the damage conditions in the concrete. The concrete region corresponding to the RC slab position and around the TC reinforcement region showed a higher level of damage than the other parts. Section 2-2, which is close to the beam column junction boundary, presented dramatically higher damage levels than section 4-4 at the center section (locations can be found in Figure 2). This difference indicated that the damage decreased rapidly as the distance from the junction boundary increased, which means that the tension load at the reinforcements was gradually shared by the infilled concrete. As the beam flange reduction increased, the peak PEEQ index increased, and the high PEEQ regions also increased. Based on the above analyses, the core concrete also participated in the load bearing, and the resulting damage level and range also increased as the flange width reduction extent increased. Therefore, for the modified through-core connections, the extent of flange width reduction needs to be controlled to avoid early and local crushing of infill concrete.

4.3. Moment Transfer Mechanism. To better understand the load sharing patterns between different components, the longitudinal force distributions at the TC reinforcements and the top beam flange and the bottom beam flange at the moment of maximum load were obtained and are compared in Figure 13. The four specimens presented similar moment transfer mechanisms, and the flange reduction had little effect on the transfer mechanism. To determine the moment transfer efficiency of the joint, the longitudinal force transfer efficiency was extracted from Figure 13. The transfer efficiency was defined as the ratio of the longitudinal force inside the tube to the force outside the tube, and detailed ratios are given Table 4. The results indicate that approximately 80% of the internal force at the bottom flange (BF) was directly transferred into the column, with less than 20% of compression force taken by the steel tube. The portion of

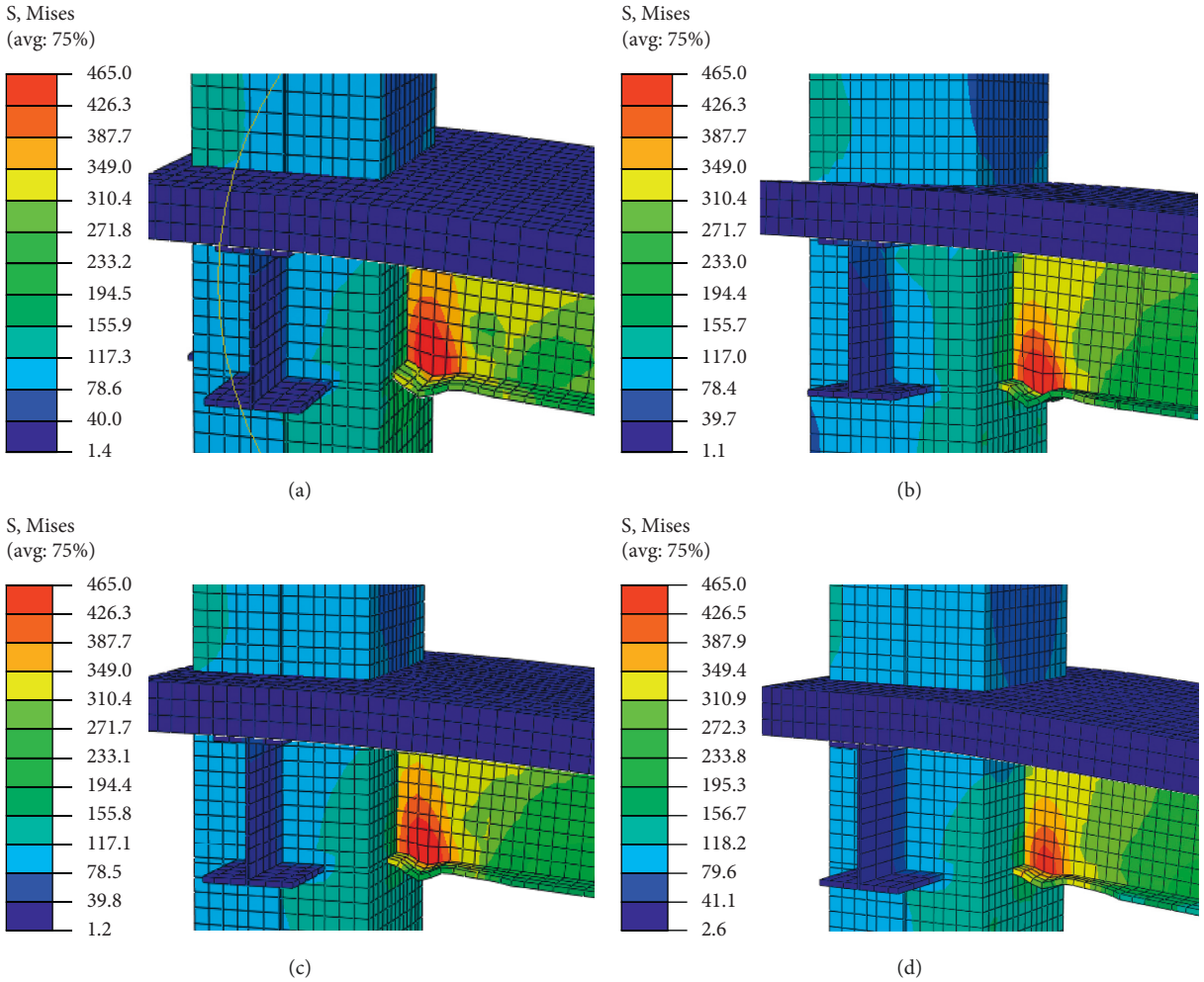

Figure 9: Failure mode by FE analysis: (a) CFCJ1; (b) CFCJ2; (c) CFCJ3; (d) CFCJ4.

load transfer directly into the column was approximately 93% at the top flange (TF) and even reached 99% at the TC reinforcements. Thus, the load transfer efficiency of the through-core connection was high.

4.4. Horizontal Shear Transferring Conditions. Figure 14 shows the horizontal shear force distribution in different components along the height of the connection region for CFCJ3. Each curve corresponds to a certain beam-tip displacement loading state, and the comparisons can reflect the load transferring variations and the horizontal shear force in the concrete. The horizontal shear force carried by the web of the steel girder did not achieve a maximum shear capacity of 576 kN under monotonic loading. This corresponded to the invisible shear failure at the joint region. In addition, the horizontal force or shear conditions at the infilled concrete displayed varied distributions as the beam end load increased. During the early loading period, the concrete core presented a more uniform horizontal force, and the maximum force occurred around the midheight of the steel girder. This horizontal force distribution resulted from the opposite tension or compression at the two flanges inside the column, leading to a type of pure shear condition in the panel zone concrete. During this period, the load shear at TC reinforcements was limited. When the connection entered the plastic state and the buckling deformation was formulated at the bottom flange, the maximum horizontal force at the infill concrete gradually moved to the locations between the top flange and TC reinforcements. The horizontal force at the infilled concrete was induced from the shear force in the panel zone and the load transmission of tension forces in the TC reinforcements to the concrete. Thus, the rapid increase of horizontal force at the concrete between the top flange and reinforcements indicated that the TC reinforcements mainly participated in load bearing and transfer after the beam yielded or buckled.

4.5. Distribution of Connection Rotation. Figure 15 shows the distribution of connection rotation between the column (θ_c), panel zone (θ_j), and beam (θ_b) from the midsection location of the column to the beam end. The results indicated that the column rotation was limited within a small level, which mainly came from the elastic bending. The majority of the connection came from the beam bending. This rotation

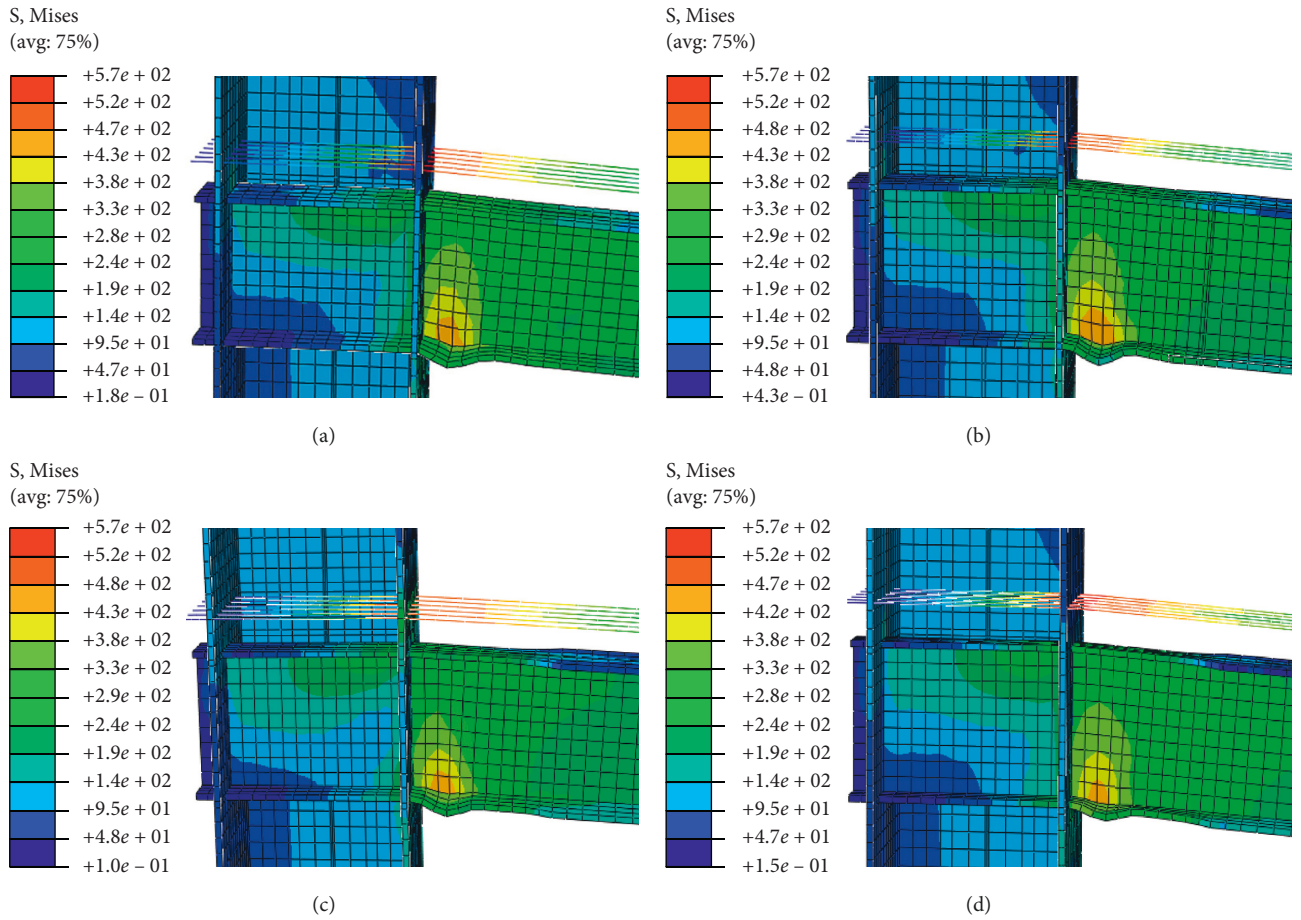

Figure 10: Stress cloud diagram for TC reinforcements and steel girder (MPa): (a) CFCJ1; (b) CFCJ2; (c) CFCJ3; (d) CFCJ4.

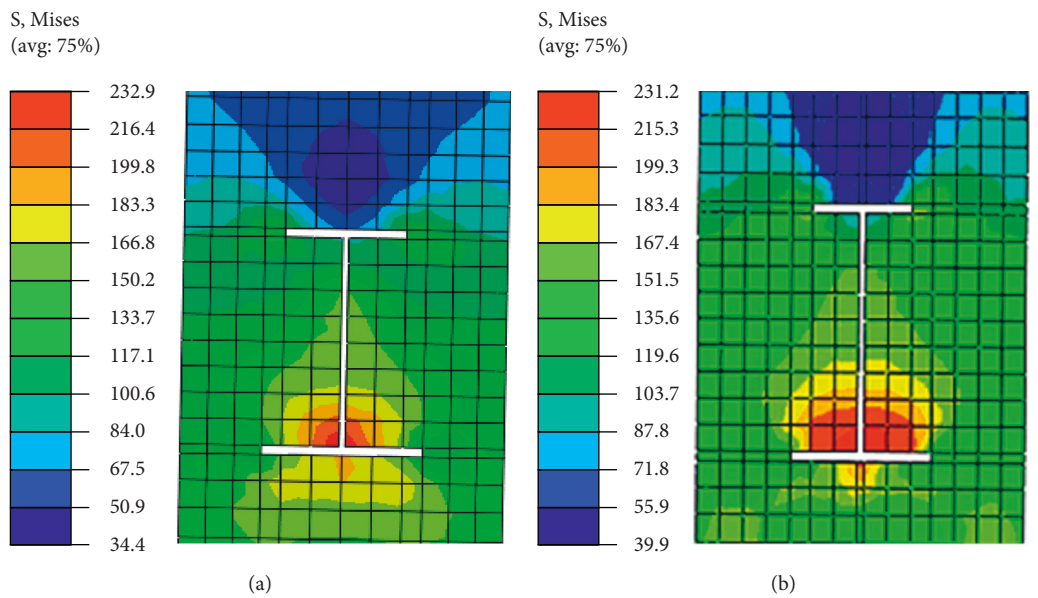

Figure 11: Continued.

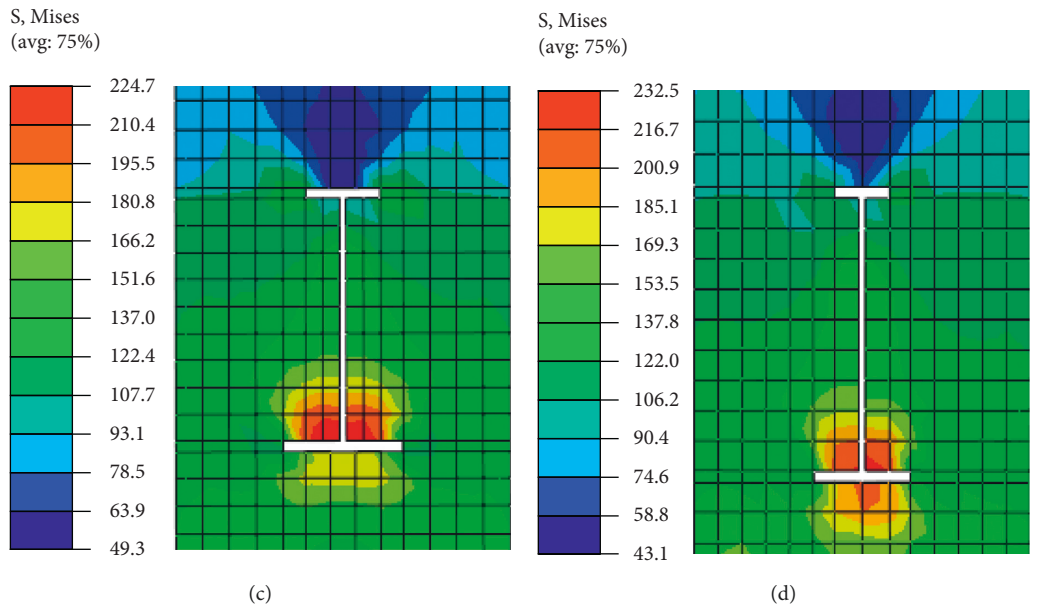

Figure 11: Stress cloud diagram for the tube (the maximum strength moment, unit in MPa): (a) CFCJ1; (b) CFCJ2; (c) CFCJ3; (d) CFCJ4.

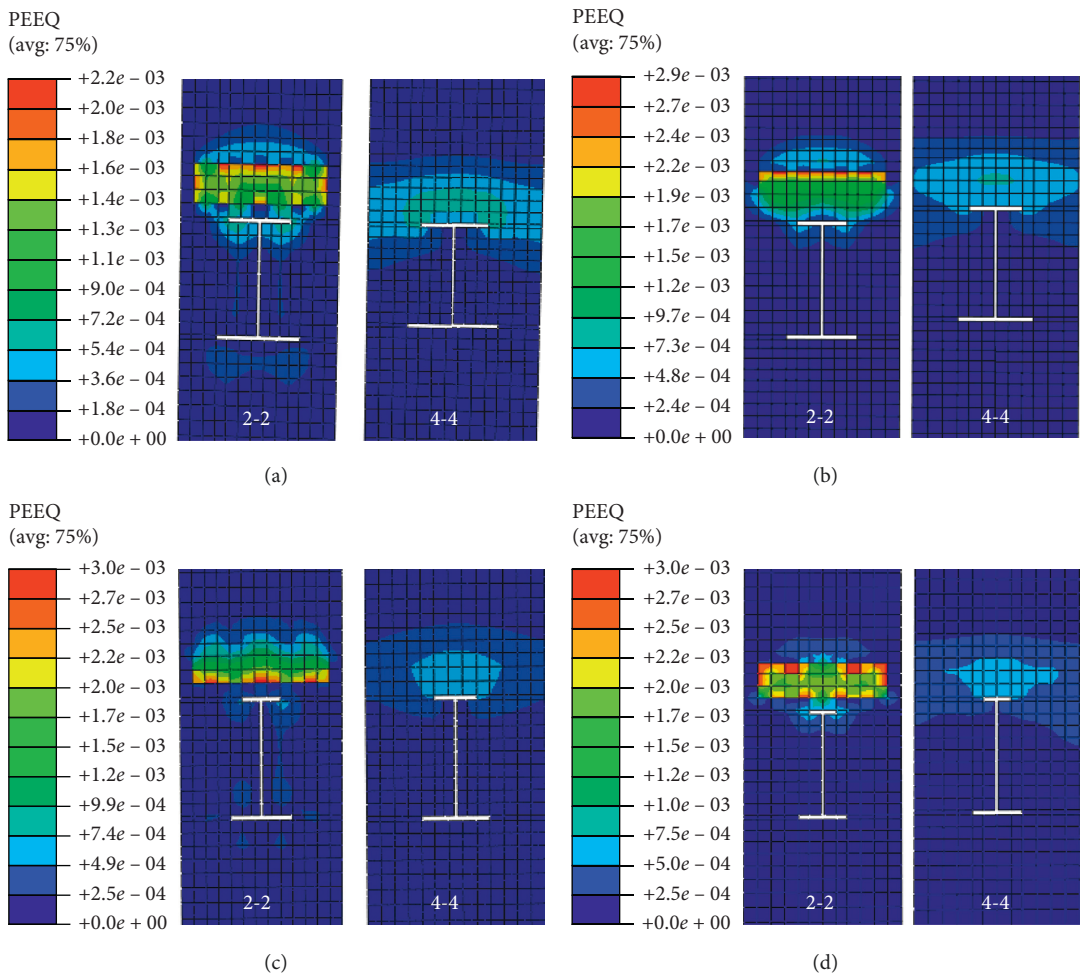

Figure 12: Equivalent plastic strain (PEEQ) of core concrete for (a) CFCJ1, (b) CFCJ2, (c) CFCJ3, and (d) CFCJ4.

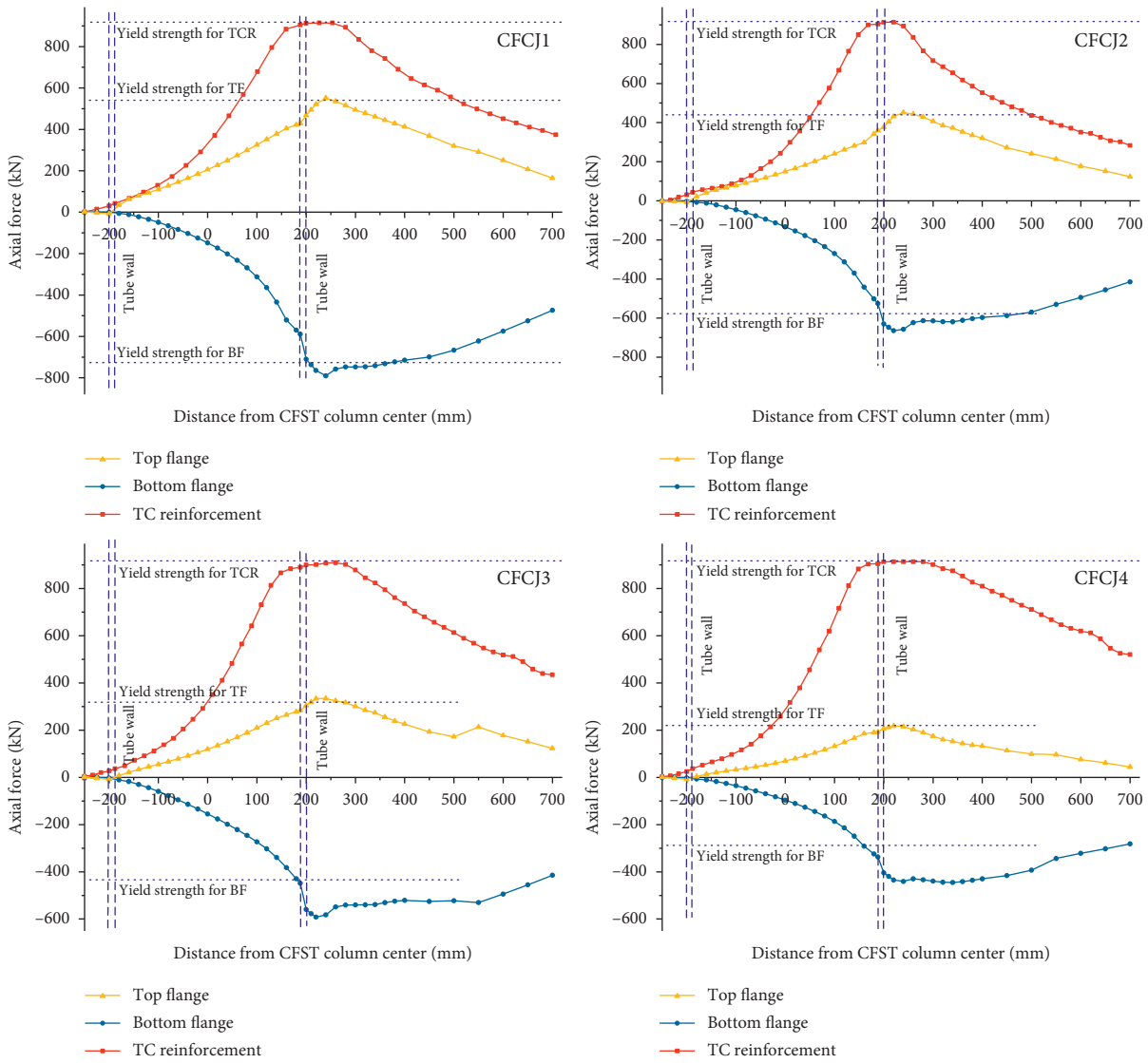

Figure 13: Distribution of longitudinal force along the beam length direction.

Table 4: Longitudinal force transferring efficiency.

	CFCJ1	CFCJ2	CFCJ3	CFCJ4	Average
TC reinforcements	0.99	0.988	0.99	0.991	0.990
Top flange	0.915	0.954	0.931	0.931	0.933
Bottom flange	0.83	0.835	0.801	0.833	0.825

development corresponded to the failure modes. Specimens CFCJ1 and CFCJ2 had a slightly uneven rotation variation at a location approximately 150 mm from the column flange (350 mm from the center of column). CFCJ3 and CFCJ4 had a more gradual rotation increase from 200 mm to 400 mm. This difference came from the difference in buckling extent, in which the specimens that had no flange reduction or a slight flange reduction presented a higher level of plastic hinge deformation and local buckling extent. In CFCJ3 and CFCJ4, the high level of flange reduction led to an increased region for plasticity development; the rotation demand at the joint was ensured through the plastic deformation in tension or compression, and the extent of local buckling was smaller.

5. Parametric Studies

The test only tested 4 specimens, with the flange reduction ratio being the sole factor. In this section, parametric studies were performed and analyzed to determine the factor influencing the pattern of flange width reduction extent, the length of reduction region, the quality of TC reinforcements, and the number of shear studs.

5.1. Flange Reduction. The above discussion indicated that the TC reinforcements in the RC slab can provide supplemental load transfer adjacent to the top flange. Then, the reduction ratio (B/A) can be set to less than 1. The test results also indicated that the connection tended to yield due to the buckling of the bottom flange, and the connection usually failed due to severe buckling deformation at the bottom

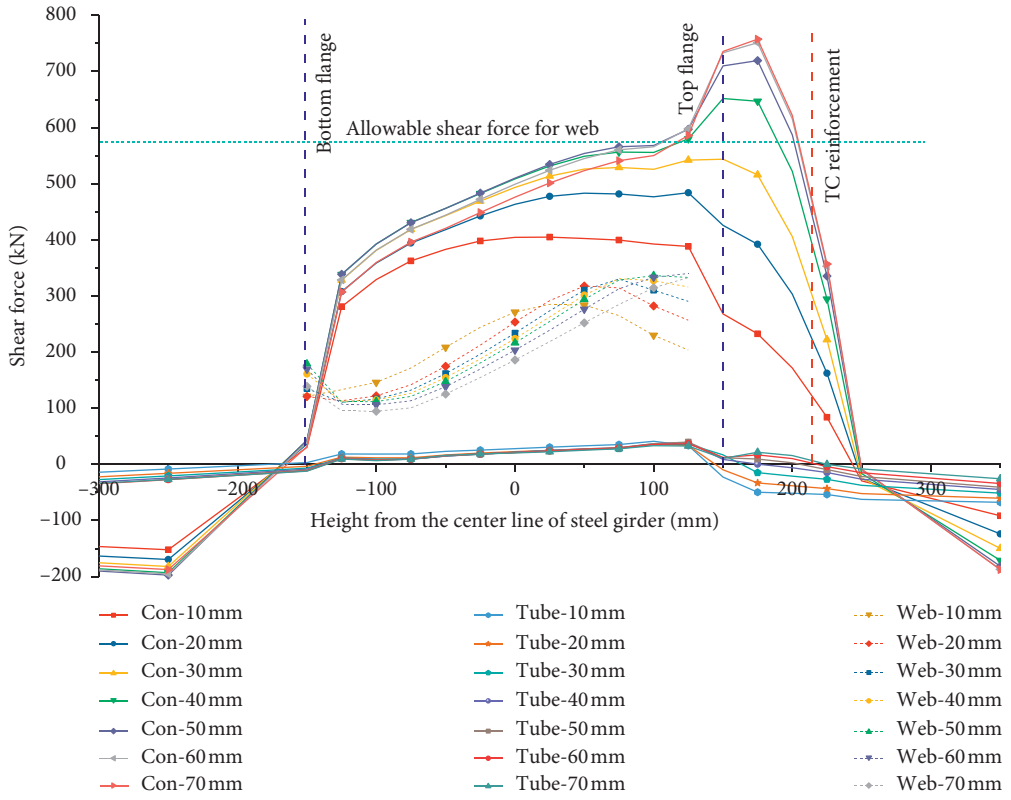

Figure 14: Shear force distribution of the joint components for CFCJ3.

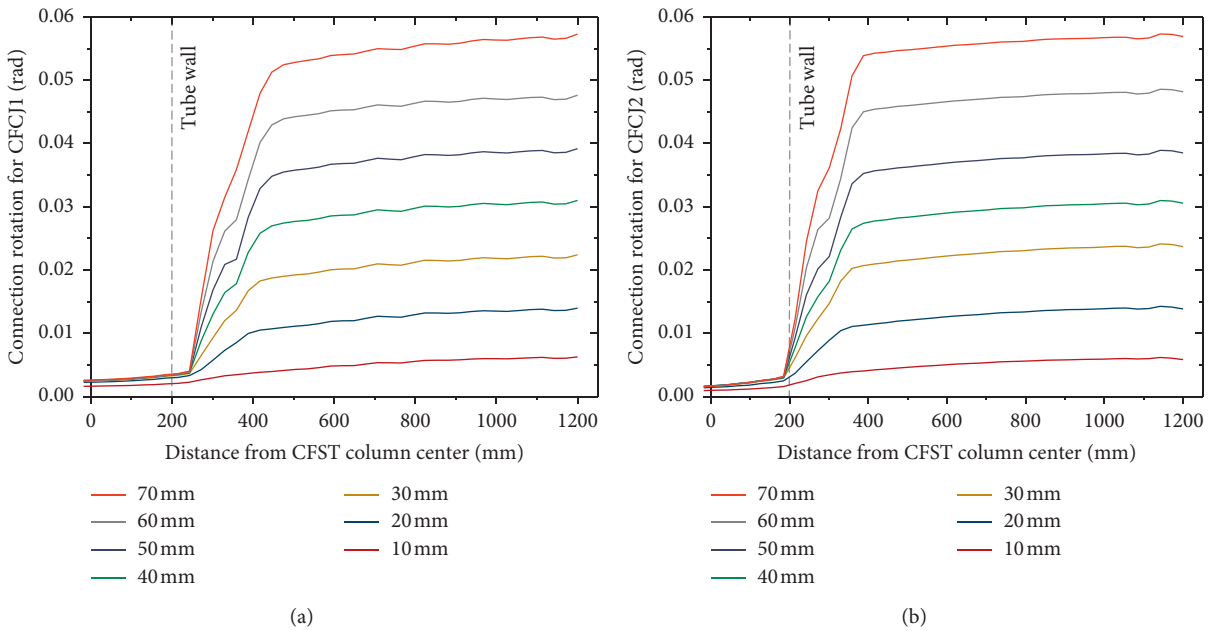

Figure 15: Continued.

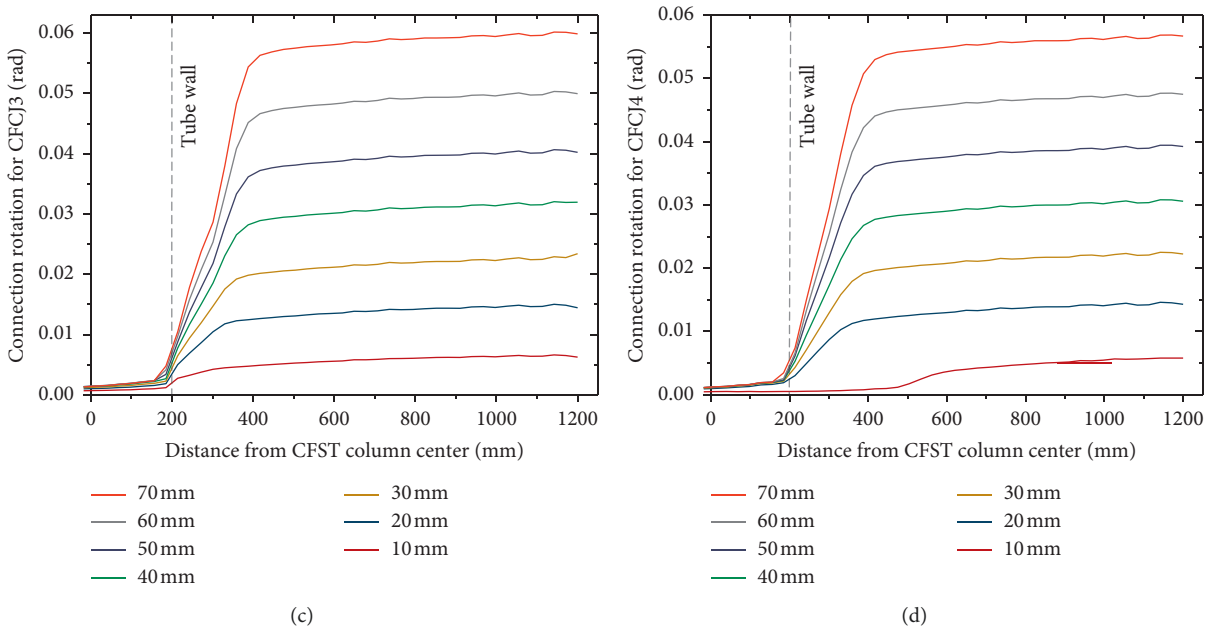

Figure 15: Distribution of connection rotation.

flange. Thus, the width reduction extent of the bottom flange (B) was more important and was closely related to the bearing capacity of the connection. Figure 16 compares the relationship of the ultimate strength capacity with the reduction degree of the bottom flange under two B/A ratio conditions. The results indicated that the ultimate capacity decreased significantly when the reduction extent exceeded 0.35. When the reduction degree surpassed 0.4, the ultimate bearing strength dropped to a lower level, and the degradation speed slowed down. Case $B/A = 1$ presented a higher strength level than the case with B/A as 0.7. Therefore, the B/A ratio was suggested to remain at a higher level, and the width reduction degree at the bottom flange was suggested to be controlled within 0.4.

5.2. Longitudinal Length of Flange Reduction. In the modified through-core connection, the beam flanges within the column region and around the joint region were all reduced. The flange width reduction region could also influence the failure mode and bearing strength of the modified connection. Then, in this section, the length of the flange reduction region was analyzed. A series of FE models were established with the length of flange reduction region l_r in Figure 2 varying from 0 to 400. Three flange reduction ratio conditions were considered under the $B/A = 0.7$ case. The comparisons are given in Figure 17. As the reduction length increased, the ultimate capacity also decreased, and the reduction speed was fast in high reduction ratio cases. When l_r surpassed 100 mm, the ultimate strength reduction speed slowed down, and the strength tended to be unchanged when l_r was larger than 200 mm. This variation can indirectly indicate that the buckling failure mainly occurred within the 200 mm length range away from the column face. When a high flange width reduction extent is needed for concrete pouring practices, the flange reduction range should be reduced to control the strength loss of the connection.

5.3. Quantity of TC Reinforcements. The TC reinforcement can effectively supply the tension load transferring in accordance with the top flange, and the affecting effect from the quantity of TC reinforcements was then investigated. The tested specimens all had 6 TC reinforcements above the top flange; then, in the FE simulations, the quantity of the TC reinforcements was varied from 0 to 10. Then, the yield strength and ultimate strength conditions were obtained and are compared in Figure 18. Compared to the joint without any TC reinforcements, the ultimate bearing capacity of 2 TC reinforcements was increased by 14.5%. Then, as the quantity of the TC reinforcement increases, both the yield strength and the ultimate strength of the connection all increased. The ultimate strength presented a higher level of strengthening effect than the yield strength. When the number of TC reinforcements was more than 8, the connection strengths stopped increasing and tended to a stable level. Since more TC reinforcements meant less space between adjacent reinforcements, the concrete bonding quality at the reinforcements would be reduced. Then, the quantity of TC reinforcements can be increased to partially increase the connection strength. However, the numbers should be controlled to ensure a minimum spacing of 25 mm between adjacent reinforcements.

5.4. Amount of Head Studs. The shear studs are in charge of the cooperative bending between the RC slab and the steel girder and the tensile deformation extent of the TC reinforcements. Thus, the effect of shear studs was analyzed and is compared in Figure 19. The parametric studies were

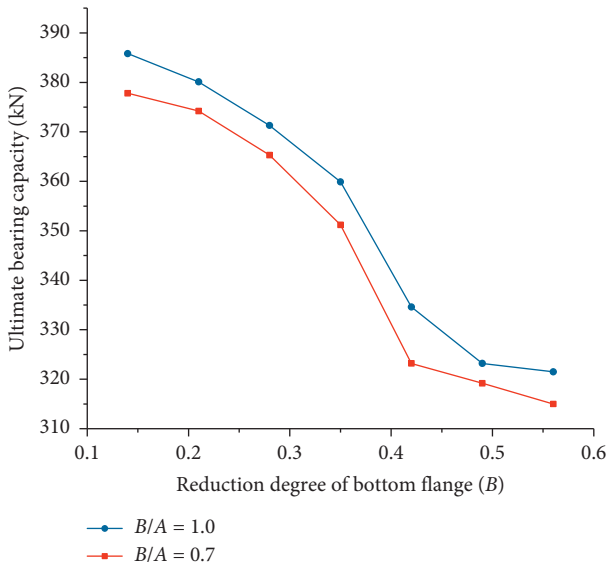

Figure 16: Effect of flange width reduction ratio.

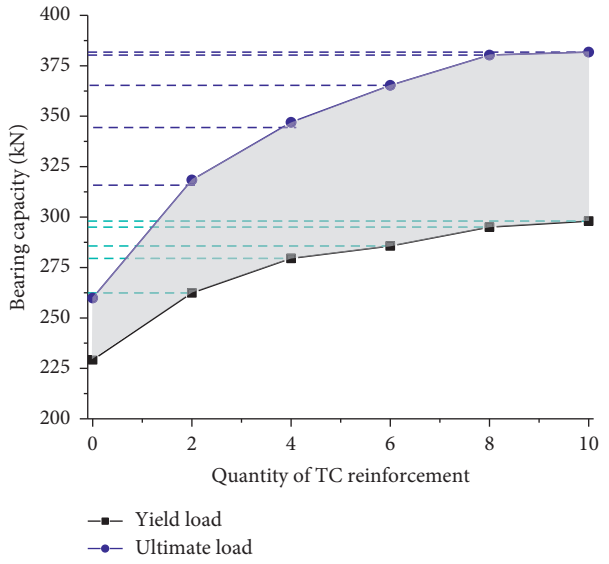

Figure 18: Effect of quantity of TC reinforcements.

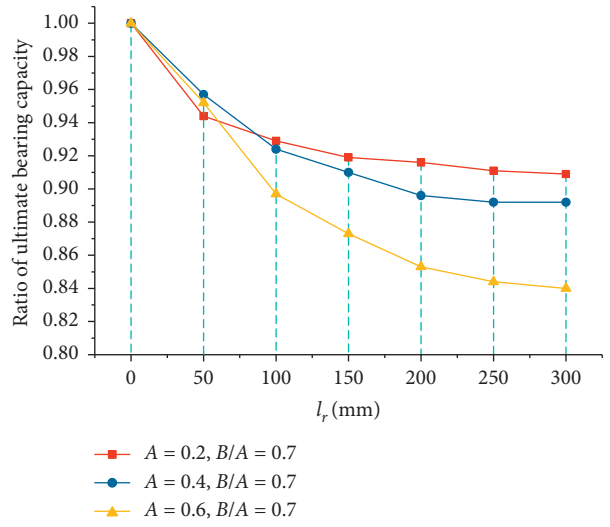

Figure 17: Comparison of the ultimate bearing capacity versus l_r.

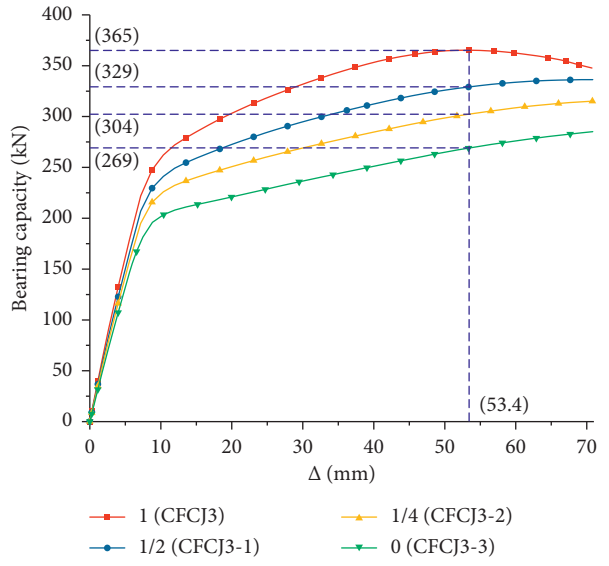

Figure 19: Comparison of the bearing capacity versus beam-tip displacement.

performed based on the CFCJ3 specimens, of which the shear stud design satisfied the full shear resistance requirements. Then, reducing the amount of shear studs to 1/2 (denoted by CFCJ3-1), 1/4 (denoted by CFCJ3-2), and 0 (denoted by CFCJ3-3) of original numbers, the applied load versus displacement relations of the 4 FE models were obtained and compared. The results indicated that the shear studs can effectively influence the load bearing capacity of the connection. With a reduced number of shear studs, the stiffness of the connection, yield strength, and ultimate strength were all reduced. The bearing capacity of the joint decreases by 9.9%, 16.7%, and 26.3% as the number of head studs was reduced to 1/2, 1/4, and 0, respectively. Due to the insufficient shear resistance between the steel girder and the RC slab, slippage occurred at the boundary, and then the composite girder effect was reduced. Thus, in the through-core connection, the number or design of shear studs must fulfill the full shear resistance requirement in composite beams.

6. Conclusion

In this paper, monotonic loading tests and FE simulations were performed on a modified through-core connection. The load bearing conditions, failure modes, cooperative working mechanism, and factors affecting patterns were carefully studied and discussed. The main conclusions can be summarized as follows:

(1) The modified through-core connections all present a plastic hinge failure at the beam end. The reduced

flange design could lead to a reduction in the yield and ultimate strength of the connection. However, even with a 40% flange width reduction, the connection can still maintain more than 85% of the connection strength. Moreover, the modified through-core connection could facilitate the convenient concrete pouring inside the column, and this connection design still possesses good performance and promising application potential.

(2) The FE method used in this paper can effectively predict the load bearing performance and working mechanism of the connection. Due to the through-core mechanism, the tension and compression force at the steel beam and TC reinforcements can be directly transferred into the column. Less than 10% tensile force at the top flange was transferred to the steel column tube, and less than 20% compressive force at the bottom flange was transferred to the tube.

(3) During the early loading stages, the steel girder took the majority load transmission portion. When the connection yielded and the plastic hinge was formulated, the load transfer at the TC reinforcements increased.

(4) The B/A ratio was suggested to remain at a higher level, and the width reduction degree at the bottom flange was suggested to be controlled within 0.4. The quantity of TC reinforcements can be increased to partially increase the connection strength. However, the numbers should be controlled to ensure a minimum spacing between adjacent reinforcements.

(5) The "longitudinal length of flange reduction" (l_r) would significantly affect the bearing capacity of the joint when varied from 0–100 mm. The shear studs were closely related to the load bearing ability and the cooperative working mechanism. During the design of the connection, the number of shear studs needed to at least fulfill the full shear resistance requirement in composite beams.

Data Availability

The data used to support the findings of this study are available from the corresponding author upon request.

Conflicts of Interest

The authors declare that they have no conflicts of interest.

Authors' Contributions

Qi-shi Zhou and Hua-wei Fu contributed equally to this work.

Acknowledgments

This research work was financially supported by the National Key R&D Program of China (Grant no. 2016YFC0701201).

References

[1] C.-C. Chen, C.-C. Lin, and C.-L. Tsai, "Evaluation of reinforced connections between steel beams and box columns," *Engineering Structures*, vol. 26, no. 13, pp. 1889–1904, 2004.

[2] Y.-J. Kim and S.-H. Oh, "Effect of the moment transfer efficiency of a beam web on deformation capacity at box column-to-H beam connections," *Journal of Constructional Steel Research*, vol. 63, no. 1, pp. 24–36, 2007.

[3] Y. Qin, Z. Chen, Q. Yang, and K. Shang, "Experimental seismic behavior of through-diaphragm connections to concrete-filled rectangular steel tubular columns," *Journal of Constructional Steel Research*, vol. 93, pp. 32–43, 2014.

[4] M. Gholami, A. Deylami, and M. Tehranizadeh, "Seismic performance of flange plate connections between steel beams and box columns," *Journal of Constructional Steel Research*, vol. 84, pp. 36–48, 2013.

[5] J. W. Park, S. M. Kang, and S. C. Yang, "Experimental studies of wide flange beam to square concrete-filled tube column joints with stiffening plates around the column," *Journal of Structural Engineering*, vol. 131, no. 12, pp. 1866–1876, 2005.

[6] A. Elremaily and A. Azizinamini, "Experimental behavior of steel beam to CFT column connections," *Journal of Constructional Steel Research*, vol. 57, no. 10, pp. 1099–1119, 2001.

[7] A. Azizinamini, Y. Shekar, and M. A. Saadeghvaziri, "Design of through beam connection detail for circular composite columns," *Engineering Structures*, vol. 17, no. 3, pp. 209–213, 1995.

[8] M. M. A. Khanouki, N. H. Ramli Sulong, M. Shariati, and M. M. Tahir, "Investigation of through beam connection to concrete filled circular steel tube (CFCST) column," *Journal of Constructional Steel Research*, vol. 121, pp. 144–162, 2016.

[9] Y. M. Alostaz and S. P. Schneider, *Connections to Concrete-Filled Steel Tubes*, Department of Civil Engineering University of Illinois at Urbana-Champaign, Urbana, IL, USA, 1996.

[10] Q.-J. Chen, J. Cai, M. A. Bradford, X. Liu, and Z.-L. Zuo, "Seismic behaviour of a through-beam connection between concrete-filled steel tubular columns and reinforced concrete beams," *Engineering Structures*, vol. 80, pp. 24–39, 2014.

[11] A. Azizinamini and S. P. Schneider, "Moment connections to circular concrete-filled steel tube columns," *Journal of Structural Engineering*, vol. 130, no. 2, pp. 213–222, 2004.

[12] Q. S. Zhou, H.-w. Fu, F.-x. Ding et al., "Seismic behavior of a new through-core connection between concrete-filled steel tubular column and composite beam," *Journal of Constructional Steel Research*, vol. 155, pp. 107–120, 2009.

[13] China Standards Press, *GB/T. 228.1-2010 Metallic Materials-Tensile Testing-Part 1: Method of Test at Room Temperature*, China Standards Press, Beijing, China, 2011, in Chinese.

[14] China Association for Engineering Construction, *CECS 159: 2004 Technical Specification for Structures with Concrete-Filled Rectangular Steel Tube Members*, China Association for Engineering Construction, Beijing, China, 2004.

[15] S. Choi, I. Shin, and C. Eom, "An experimental study on the strength and stiffness of concrete filled steel column connections with external stiffener rings," in *Proceedings of the 4th Pacific Structucal Steel Conference*, pp. 1–8, Pergamon, Singapore, October 1995.

[16] L. Luo and X. Zhang, "Flexural response of steel-concrete composite truss beams," *Advances in Civil Engineering*, vol. 2019, Article ID 1502707, 15 pages, 2019.

[17] F. Ding, X. Ying, L. Zhou, and Z. Yu, "Unified calculation method and its application in determining the uniaxial

mechanical properties of concrete," *Frontiers of Architecture and Civil Engineering in China*, vol. 5, no. 3, pp. 381–393, 2011.

[18] F.-X. Ding, J. Liu, X.-M. Liu, F.-Q. Guo, and L.-Z. Jiang, "Flexural stiffness of steel-concrete composite beam under positive moment," *Steel and Composite Structures*, vol. 20, no. 6, pp. 1369–1389, 2016.

[19] F.-x. Ding, Z. Li, S. Cheng, and Z.-w. Yu, "Composite action of octagonal concrete-filled steel tubular stub columns under axial loading," *Thin-Walled Structures*, vol. 107, pp. 453–461, 2016.

[20] J. Ollgaard, R. Slutter, and J. Fisher, "Shear strength of stud connectors in lightweight and normal weight concrete," *AISC Engineering Journal*, vol. 8, no. 2, pp. 55–64, 1971.

[21] AIoS Construction, *AISC 360-Specification for Structural Steel Buildings*, AIoS Construction, Noida, India, 2005.

[22] Dassaults Systems Simulia, *ATCAE Abaqus Handbook for User*, Dassaults Systems Simulia, Johnston, RI, USA, 2005.

[23] Q. Su, X. Du, C. Li, and X. Jiang, "Tests of basic physical parameters of steel concrete interface," *Journal of Tongji University*, vol. 44, no. 4, pp. 499–506, 2016.